Eur Radiol (2005) 15: 2172–2184
DOI 10.1007/s00330-005-2829-3

Peter D. Gatehouse
Jennifer Keegan
Lindsey A. Crowe
Sharmeen Masood
Raad H. Mohiaddin
Karl-Friedrich Kreitner
David N. Firmin

Applications of phase-contrast flow and velocity imaging in cardiovascular MRI

Received: 11 May 2005
Accepted: 31 May 2005
Published online: 8 July 2005

P. D. Gatehouse · J. Keegan · L. A. Crowe · S. Masood · R. H. Mohiaddin · D. N. Firmin
Royal Brompton Hospital and National Heart and Lung Institute, Imperial College, London, UK

K.-F. Kreitner
Klinik und Poliklinik für Diagnostische und Interventionelle Radiologie, Johannes Gutenberg-University, Mainz, Germany

P. D. Gatehouse (✉)
Cardiovascular MRI Unit, Royal Brompton Hospital, Sydney Street, London, SW3 6NN, UK
e-mail: p.gatehouse@rbh.nthames.nhs.uk
Tel.: +44-20-73518807
Fax: +44-20-73518816

Abstract A review of cardiovascular clinical and research applications of MRI phase-contrast velocity imaging, also known as velocity mapping or flow imaging. Phase-contrast basic principles, advantages, limitations, common pitfalls and artefacts are described. It can measure many different aspects of the complicated blood flow in the heart and vessels: volume flow (cardiac output, shunt, valve regurgitation), peak blood velocity (for stenosis), patterns and timings of velocity waveforms and flow distributions within heart chambers (abnormal ventricular function) and vessels (pulse-wave velocity, vessel wall disease). The review includes phase-contrast applications in cardiac function, heart valves, congenital heart diseases, major blood vessels, coronary arteries and myocardial wall velocity.

Keywords MRI · Cardiovascular · Blood flow · Phase contrast · Velocity mapping

Introduction

MRI in cardiovascular blood flow has a range of established applications, especially in congenital heart disease and heart valves [1, 2], and many other interesting research applications which may soon become clinically useful. This review covers the main MRI method for measuring blood and myocardial motion, called phase-contrast imaging, velocity mapping, flow imaging, etc.; unfortunately, MRI names vary! Alternatively, MRI can label material and image its subsequent motion, but this approach was superseded for bulk blood flow by the more reliable phase-contrast method. Phase-contrast MRI of blood flow is non-invasive, without ionising radiation and can measure flow accurately [3–5], with flexibility of image spatial and temporal resolution to suit the application, and has access to all directions of flow at any location in the body. Similar velocity-encoded data are collected for phase-contrast angiography, which uses a different reconstruction method and produces flow-enhanced images [6].

MRI is difficult to use on patients with life-support apparatus because of projectile and interference hazards near the magnet. Open-access MRI scanners alleviate some difficulties, but reduce imaging performance. Most cardiac MRI requires breath-hold co-operation for collecting raw data over several cycles, to be combined into high-reso-

lution images. Consistent cardiac timing in each cycle is assumed, and can be adversely affected by cardiac arrhythmia. Some "retro-gated" techniques correct abnormal cardiac intervals while scanning.

On whole-body MRI systems, blood flow is imaged in the heart chambers and blood vessels with diameters greater than about 3–4 mm. In the main circulation, blood flow is complicated, it does not flow evenly at the same speed at all points across a vessel, let alone the powerful effects of cardiac pulsatility. Blood flow has many parameters; e.g. the total volume of blood per cardiac cycle or per minute, the mean velocity over the vessel area, or averaged over the time of a cardiac cycle; the shape of the velocity distribution over the vessel area ("flow profile"), or again during time through the cycle ("flow or velocity waveform") (again, the terms are not standardised), and the amount of turbulent flow, which is small in normal circulation. As a general introduction to MRI phase-contrast velocity measurement, typical in-plane image pixel sizes vary, from about 0.2 mm (peripheral and carotid vessels) to about 2–3 mm (deep vessels and heart chambers) at temporal resolutions (but averaged over multiple cardiac cycles) typically 20–70 ms, but capable of 2 ms for pulse-wave applications. Most of this article's references show recent progress and are based on much older original research investigations.

Fundamental basis

MRI is usually displayed as magnitude (modulus) images: brighter pixels contain more signal. The signal is from the rotating transverse magnetisation in the pixel, which is a vector quantity (two properties: size and direction). Although the direction is rotating, MRI detects how far it is running ahead or behind a reference rotating source (oscillator) in the scanner electronics. This ahead or behind quantity is known as phase (phase shift), used for position encoding in MRI because the magnetic field gradients cause phase shifts depending on position-and also on velocity. Phase has a 360° range, beyond which the same values repeat, causing wraparound (aliasing). The phase of each pixel is affected by uncontrolled factors like main field nonuniformity and chemical shift, so the phase reconstruction (phase image) is not normally displayed.

Velocity-encoding

For phase-contrast, two opposing gradient pulses known as velocity-encoding are added to the imaging sequence of pulses. In pixels containing static tissue, the effects of the two pulses cancel, but if the tissue moves in the time between the pulses, they leave a phase shift in that pixel accurately proportional to velocity along the gradient's direction. The uncontrolled phase errors must be removed to detect only the velocity phase shift, so two scans [typically "reference" and "velocity-encoded (sensitized)"] are usually acquired together (Fig. 1). Subtracting the reference phase image from the velocity-encoded phase image makes the phase-contrast image (velocity map). The sensitivity and direction of velocity-encoding is flexible and can be repeated for multi-directional velocity imaging. Stationary material is mid-grey (zero-value pixels), with increasing velocities in opposite directions shown brighter (positive pixels) and darker (negative pixels), with an accurate linear relationship to velocity, i.e. velocity in pixel= VENC×(pixel phase shift/180°), and labelled with direction rather than the ± sign. The velocity encoding value VENC should be available as an adjustable sequence pa-

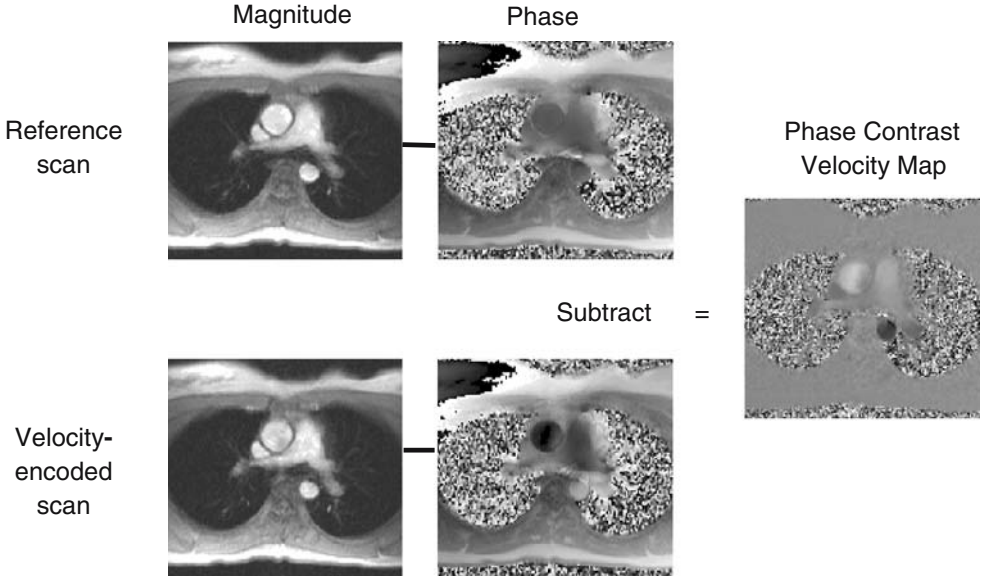

Fig. 1 Magnitude and phase images are reconstructed from the reference scan (*top row*) and also from the velocity-sensitive scan (*bottom row*). The phase images are subtracted to make the phase contrast image (*velocity map*)

rameter. A small VENC represents a highly velocity-sensitive image.

Velocity aliasing or wraparound

If the velocity phase shift exceeds ±180° (Fig. 2), it cannot be distinguished from one within the ±180° range, which is displayed instead and known as velocity aliasing (wraparound). Although the measurable range of velocity phase shifts is always 360°, i.e. 2×VENC, it can be offset in post-processing so that aliasing does not affect the region of interest (ROI) (Fig. 2b). If the true range of velocities in the ROI exceeds 2×VENC, they cannot all be correctly displayed simultaneously; peak velocity may still be found, but mean velocity and flow will be more difficult. Some inaccuracy in VENC amount and direction occurs in distorted gradient fields [7]. After acquisition, VENC cannot be changed, so on-line assessment of the velocity images is necessary, and if aliasing appears excessive, repeated with larger VENC. Unhelpful software often forces users to avoid any aliasing, by using excessively large VENC, at less obvious cost of lower velocity-noise ratio. Quicker low-resolution images can be helpful for optimisation. (Narrowing the display greyscale "window width" does not alter VENC range, and "window level" is often not linked to VENC offset, but causes high-velocity pixels to "saturate" the display greyscale full black and white. Note that velocity pixel values may be uncalibrated in images displayed other than by using the dedicated flow processing software).

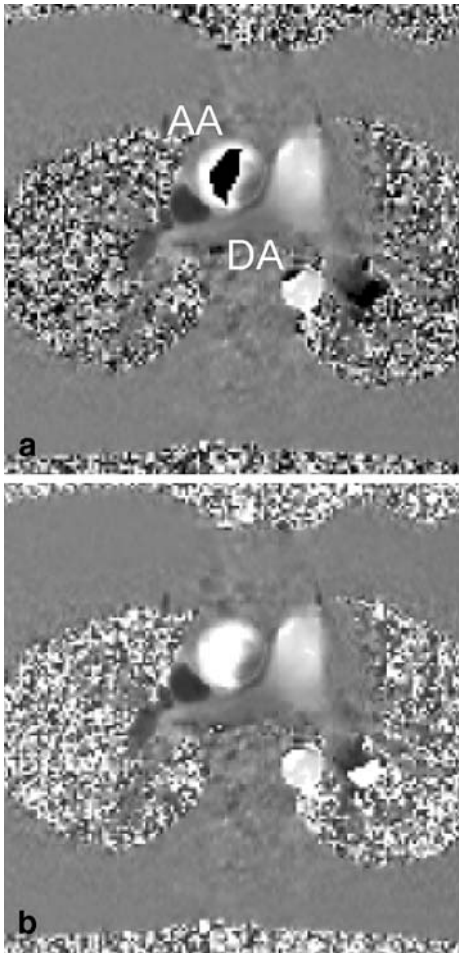

Fig. 2 Velocity wraparound: unaliased flow towards the head is *white*, to the feet is *black*. (**a**) Systolic flow in the ascending aorta (*AA*) and the descending aorta (*DA*) exceeds the 80 cm/s VENC, corrected for the AA in (**b**) by offsetting the velocity range (now 30 cm/s to feet=*black*, 110 cm/s to head=*white*). Wraparound in flow towards the feet increased in (**b**) but can be corrected separately

Pulse sequences for phase-contrast

Phase-contrast requires a strong signal from fast-moving blood, using spoiled gradient-echo sequences with velocity-compensation (even-echo rephasing) and short echo-time (TE), running with cardiac gating as a cine acquisition using reduced flip angle. For imaging within a single breath-hold, the sequence usually collects multiple raw-data lines per cardiac cycle (i.e. segmented acquisition). The repeated RF pulses for multiple raw data lines per cardiac cycle require further reduced flip-angle and therefore lower signal-to-noise ratio. On some systems, high-strength gradient pulses worsen eddy-current effects on the stationary offset, improved by repositioning the patient for each vessel measured to be as near isocentre as possible, and using lower gradient performance (with consequential spatial and temporal resolution losses). A smaller VENC value requires more velocity-encoding strength and duration within the TE, which can conflict with the short TE required in turbulent flow and the short repeat time for segmented imaging. Using the ECG, images are usually repeated at each cardiac-phase for phase-contrast cines. Reference magnitude images show bright systolic blood, enhanced by inflow of unsaturated blood, with little ghosting from blood, due to the velocity-compensation. In the velocity-encoded measurement, the velocity-encoded direction is clearly not completely velocity-compensated. Magnitude images from the velocity-encoded measurement may therefore show signal loss or flow ghosting artefacts in complex or time-varying flows (Fig. 4c). The earliest cardiac cine image may be delayed by the ECG-filtering and communication of R-wave trigger detection through the MRI system to the sequence, and also, in segmented imaging, acquisition of central raw-data after typically half of the cine frame time. For faster imaging, data sampling may best use "centre-out" EPI [8] or spiral [9], with short sampling durations after each RF excitation for turbulent flow. Phase-contrast sequences can also be accelerated by parallel RF [10] and shared-cine-phase [11] methods. The re-use of transverse magnetisation in bal-

anced SSFP [12] does not combine easily and flexibly with velocity encoded phase shifts, but the bright blood signal has attracted some initial investigations for phase-contrast.

Phase-contrast image processing

Truly empty pixels appear as "speckle", since the phase-shift of low-amplitude noise is random. Ghosting along the phase-encode direction in phase-contrast images, sometimes with a large phase shift, corresponds to even a very weak ghost in the magnitude image (Fig. 3). Both effects in phase-contrast images can be zeroed in pixels whose magnitude image value falls below a user-specified "magnitude threshold" in post-processing. If the flow of interest in the magnitude image is bright, its phase is not significantly affected by ghosting with relatively weak signal magnitude. However, especially in slow flow where signal magnitude is low, ghosting may become problematic, and random noise also causes phase deviations which appear as noise on pixel velocity values ("velocity-to-noise ratio"); VENC should be small so that the velocity phase shift is large relative to the random noise, but a small VENC also tends to increase flow ghosting in the velocity-encoded image.

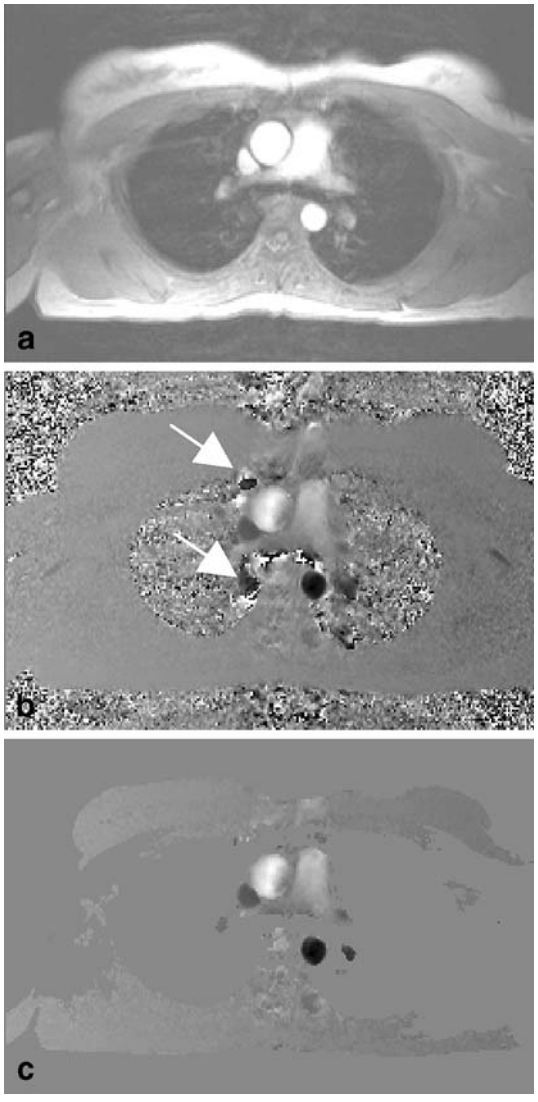

Fig. 3 Respiratory ghosts with weak magnitude (**a**) can appear strongly in phase-contrast image (**b**) (*arrows*, probably also by respiratory variation in venous flow). Ghosting and random-phase empty pixels are suppressed using magnitude thresholding (**c**). Also, an uncorrected static tissue offset varies across the image

For various reasons (uncorrected Maxwell, eddy currents, small gradient waveform errors), all tissue may show a small erroneous velocity, which may be uniform or vary (linearly or curvedly) across the image (Fig. 3c). Processing software may allow users to place a correction ROI in stationary tissue, preferably near the vessel being measured; the correction ROI value is subtracted from the vessel velocity. Another approach requires the user to identify stationary tissue all over the FOV (avoiding phase-encode wraparound!) and fits a correction slope which is then subtracted from all pixels for a corrected velocity image. Low SNR in limited amounts of nearby stationary tissue can make background correction difficult to achieve accurately. Phase-contrast images should correct Maxwell (concomitant) errors [13].

Spatial resolution and image plane alignment

For mean velocity in a vessel, accurate lumen area delineation demands high in-plane resolution. At least four true pixels are needed (not interpolated or zero-filled!) across the vessel diameter in both directions for 10% accuracy [3, 14]. The situation is complicated by varying partial volume effects at the edges of the flow, due to surrounding tissue signal level, the type of flow near the vessel boundary (laminar or plug flow), and misalignment of the usually thicker slice than in-plane resolution, so high spatial resolution and thin slice thickness are important. Volume flow measurement is not affected by including zero-velocity pixels, allowing easier ROI definition if magnitude thresholding is used.

If velocity-encoding is misaligned by angle θ from the flow direction, the measurement gives the true velocity× cos(θ). However, this error is small, e.g. 6% at 20° misalignment, and for flow measurements is cancelled by 1/cos(θ) increase in apparent cross-sectional area. The voxel dimensions and their alignment with flow are also important where a voxel may contain a range of velocities. In the velocity-encoded measurement, such a voxel contains a range of phase-shifts and its total signal can be inaccurate [15] or lost altogether, even if it is strong in the reference magnitude image. This effect is concealed when the velocity-encoded images are not available. It may be im-

proved by larger VENC to reduce intra-voxel velocity phase dispersion, but this worsens velocity-to-noise ratio [15].

Temporal resolution

Breath-hold imaging collects multiple lines of raw data for each cine frame in each cardiac cycle, and the cine frame is extended further for velocity mapping by the collection of reference and velocity-encoded data within the same cycle, as opposed to sequential collection on successive cardiac cycles which extends breath-hold time. Highly pulsatile velocity waveforms may be smoothed, but accuracy is retained by cine frames less than 60–70 ms [16], longer if the flow is less pulsatile [17], and smoothing might sometimes have less effect on mean flow measurements [18]. Flow in smaller vessels also loses accuracy because the breath-hold time limits spatial resolution and further if they move during the cine frame [19]. Breathing patterns can alter cardiac function and flow [20, 21]. Using slower non-breathhold imaging may average such variations, but introduces respiratory artefacts (Fig. 3).

Misregistration of flow data

Time differences of a few milliseconds occur between the measurements of position and velocity in the phase-contrast scan, which can misregister oblique flow compared with static tissue [22]. Although partly correctable in sequence design, the remaining "encoding time scatter" can also distort accelerating flow [23]. In velocity maps, phase errors caused by changing velocity reduce with shorter TE [22], but acceleration into stenoses requires caution [24].

Methods of applying phase velocity mapping

Volume flow measurements

The volume of blood flow in a vessel per cardiac cycle is measured using through-plane velocity encoding in a cine acquisition. The measurement should avoid temporal smoothing of flow pulses (i.e. use fine temporal resolution). If late diastolic flow is negligible, ECG-triggered cine MRI may be used. "Retrospective ECG" or "retrogating" acquires the whole cardiac cycle, and may stabilise stationary offset error. The flow volume per cardiac cycle is the sum of the velocities of the pixels within the ROI multiplied by the area at each cine frame. The ROI around the blood vessel in each frame may require re-drawing for motion and vessel compliance during the cycle. If pixels surrounding the vessel contain so little signal that they show random phase speckle, their inclusion causes errors. The stationary offset error is more significant in comparison to the slower flow often occurring during large fractions of the cardiac cycle, which can be improved by varying VENC for those frames [25], a method infrequently used, perhaps due to its extra complexity.

Cardiac output is available from phase-contrast. For assessment of left ventricular output, the imaging plane in the ascending aorta should be at a level of the bifurcation of the pulmonary trunc (Fig. 4a). A common alternative is to use SSFP cine "volumetry", which also measures ejection fraction and myocardial mass, and provides some information on myocardial motion. However, this alternative is limited in the presence of valvular regurgitation. Many types of cardiac shunt are measured by the pulmonary-to-systemic ratio (Qp/Qs), comparing MRI flow measurements in the pulmonary trunk and proximal aorta [26]. This method shows high accuracy compared with other methods, such as catheter oximetry [27], potentially improved by additional data from biventricular cine volumetry. Flow imaging can be applied directly to the shunt [28], to find the total volume flow, study its velocity-time waveform or simply to find its direction. Direct measurement of the shunt flow requires careful slice positioning if it moves during the cardiac cycle.

Volume flow measurement by MRI is also applied to measure the amount of collateral flow around obstructions such as aortic coarctation (see below) or the severity of valve regurgitation by measuring the reverse flow [29, 30, 43]. Particularly in the latter application, the effect of stationary offset error can be severe, and can be checked by imaging a stationary phantom with identical sequence and image plane settings soon after the patient study. Valve regurgitation flow measurement can miscount valve plane motion [31] and compliance volume changes [32] as flow through the valve, improved using a moving slice method [33] (Fig. 5).

Stenotic flow

The aim is to measure the severity ("hemodynamic significance") of a stenosis. Subject to several assumptions [34], this appears as a pressure drop through the stenosis (in medicine called a pressure gradient, confusingly). Blood leaves the stenosis in a narrow systolic "jet" of fast flow which disperses downstream. The stenotic pressure gradient (in mmHg)=4× the peak jet velocity (m/s) squared, by the "modified Bernoulli equation", assuming that the upstream velocity is small compared with the jet peak velocity, and that the stenosis obstructs about 70–80% by diameter of the vessel. The factor 4 can be varied according to stenosis diameter measurement [34, 35]. Reliable jet signal requires short echo time (TE<4 ms) and velocity compensation [36]. Signal loss around the jet is expected, but the peak velocity in the jet can be measured in a small ROI of only a few pixels-with careful positioning, because the jet velocity varies along and across the jet. Cross-sec-

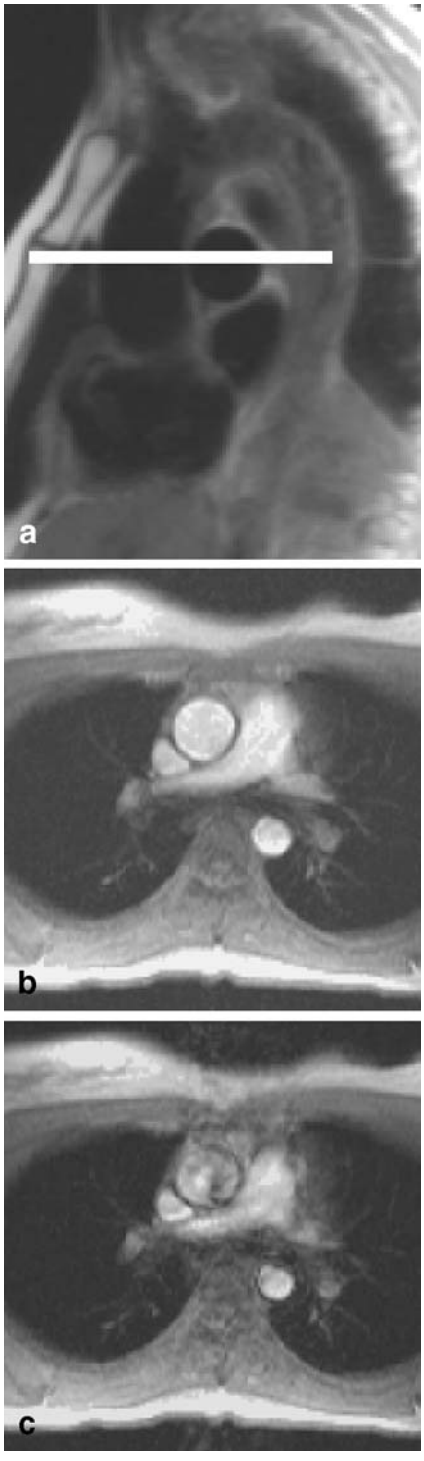

Fig. 4 (**a**) Planning level for assessment of left ventricular output in the ascending aorta. The reference image (**b**) and velocity-encoded image (**c**) at the same systolic cardiac timing. Velocity-encoding causes signal loss and ghosting from complex flow. Pixels with signal loss in the velocity-encoded image may give unreliable phase-contrast velocity data

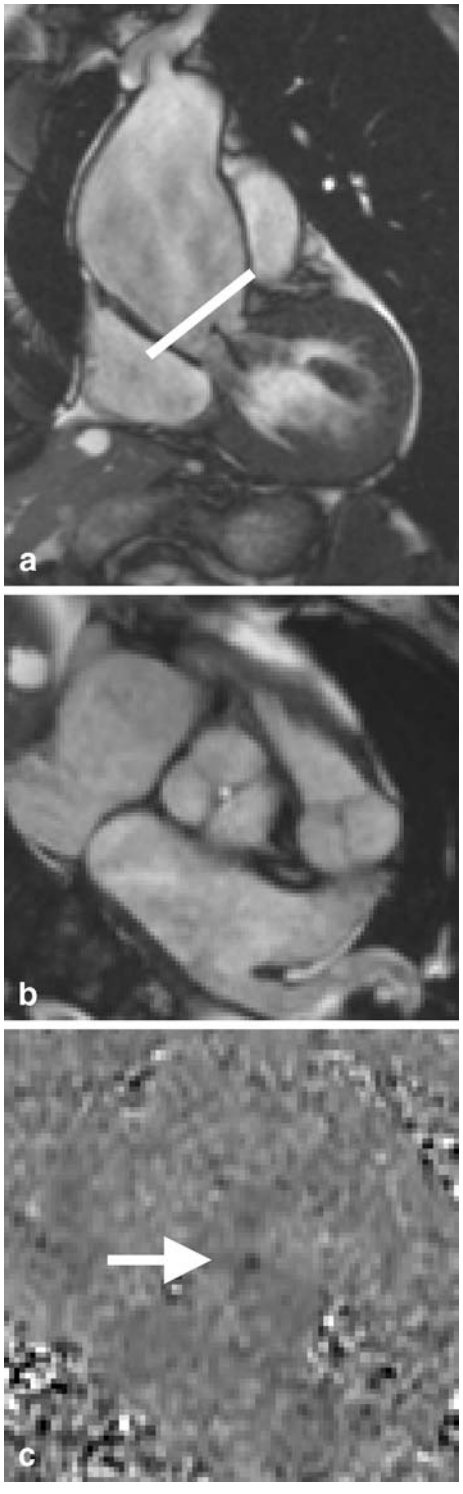

Fig. 5a–c Aortic valve insufficiency in a patient with aneurysm of the ascending aorta and consecutive widening of the aortic annulus. **a** Planning of the phase-contrast measurement with through-plane velocity-encoding in a cine frame. **b** Documentation of the insufficient closure of the aortic leaflets on a cine image. **c** Diastolic frame from phase-contrast cines with through-plane velocity-encoding indicating retrograde flow in end-diastole (*arrow*)

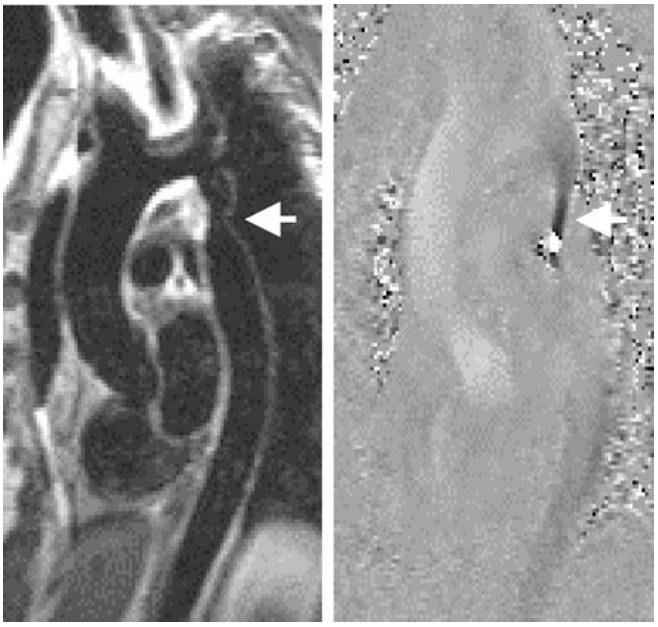

Fig. 6 Aortic recoarctation. Significant narrowing at the site of a previous coarctation repair (*arrow*) on the anatomical image (*left*). The corresponding systolic phase contrast image (*right*) shows a tight stenotic jet with velocity aliasing at 4 m/s VENC. Flow towards the head is *white*, to the feet is *black* but aliases to *white*

tional imaging perpendicular to the jet using through-plane velocity encoding should be located correctly along the jet for the peak. For in-plane velocity encoding along the jet using a thin slice, preferably narrower than the jet, the selected slice must be aligned with the jet axis to avoid underestimation. Typically, several "cross-cutting" in-plane and through-plane velocity images are obtained to ensure peak detection [2]. Avoiding pixels affected by signal loss or misregistration, especially by viewing the velocity-encoded magnitudes, overestimating the peak velocity is unlikely. Applications of peak velocity measurement include aortic coarctation (Fig. 6) and valve disease (Fig. 7). For coarctation [1, 37], MRI can also measure the collateral flow by comparing aortic flow measurements immediately distal to the stenosis with flow measured further downstream after vessels carrying collateral flow have rejoined the aorta, or use contrast-enhanced MRA. In valve disease [38], movement of the valve during the cardiac cycle would best be followed using slice-tracking [33], or the slice located correctly for the time of the relevant flow. As well as flow [30], signal loss in magnitude images is used to assess stenosis, since turbulent signal loss is small in normal circulation.

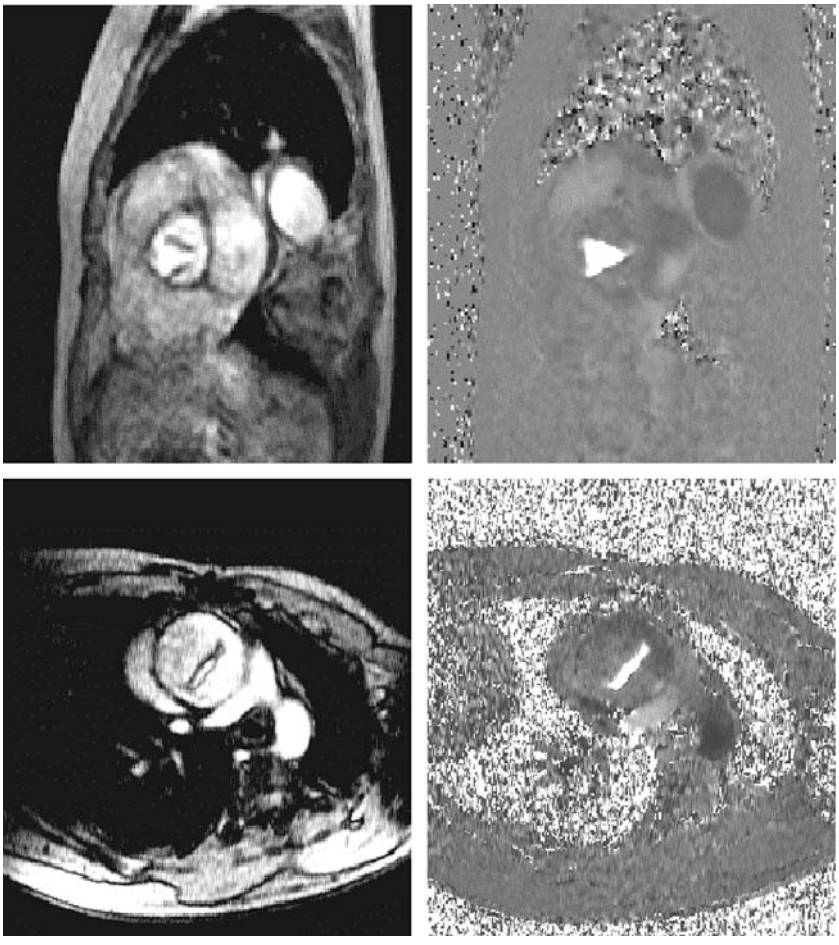

Fig. 7 Trileaflets aortic valve (*upper panel*) and stenotic bicuspid aortic valve (*lower panel*). Systolic frames from phase-contrast cines (*left* magnitude, *right* velocity) with through-plane velocity-encoding. Fast-moving blood into the page is shown *white*. The velocity image shows the cross-sectional area of the valve opening and also the peak velocity for pressure gradient assessment

Flow as a source of image contrast

Fresh inflow of fully magnetized blood enhances signal brightness in short TE spoiled gradient-echo cine images, while the magnetisation of static or slow-moving material is reduced by the repeated RF pulses ("saturation"). Either this flow enhancement or through-plane velocity images can be used to assess the cross-sectional area of a flow, such as an atrial septal defect [39] or valve opening area (Fig. 7). When using magnitude image signal loss to assess turbulence, the robust signal at short TE becomes a drawback, which can be specially adapted for this purpose [40]. In balanced-SSFP imaging, fresh-inflow enhancement is not expected, and spurious flow-brightening and signal loss effects are less well-controlled than in spoiled gradient-echo imaging [41]. Phase-contrast provides image contrast by differing flow patterns and timings, e.g. the true and false lumina in aortic dissection [42, 43] (Fig. 8).

Velocity waveforms and flow patterns

At sufficiently fine temporal resolution, phase-contrast MRI detects abnormal blood velocity waveforms during the cardiac cycle, e.g. the shorter acceleration time caused by increased pulmonary vascular resistance [44]. The pattern of mitral in-flow [45] shows abnormal ventricular filling, where the ratio of two diastolic flow peaks (E/A ratio) changes, possibly another application for real-time imaging while breathing. The full cardiac cycle coverage of retrospectively-gated MRI improves coverage of atrial contraction and venous flow, but the combination of data from multiple cardiac cycles remains sensitive to diastolic variability. In renal artery stenosis, the reduced systolic peak in the velocity waveform may be a useful addition to mean flow measurement [46]. Velocity waveforms contain information about vessel compliance and the returning pressure wave from downstream [47], a topic of great complexity possibly affecting coronary artery flow [48].

Complete acquisition of a complex pulsatile flow requires cine phase contrast in three directions and three dimensions (Fig. 9). Ideally using respiratory gating, the acquisition time is at least 20 min accepting some resolution loss [49, 50]. Dedicated acquisition and display software is usually needed. Complete flow acquisitions

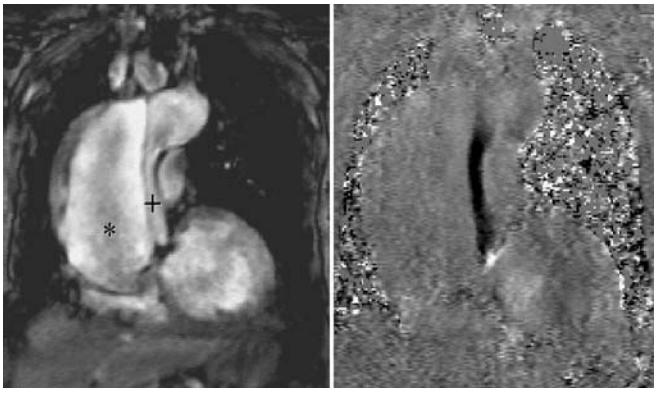

Fig. 8 Gradient echo image (*left*) and the corresponding in-plane velocity-encoding (*right*) in a patient with type A aortic dissection. Flow (*black*, upward on the velocity image) is found in the true lumen (+) with relatively stationary blood in the false lumen (*)

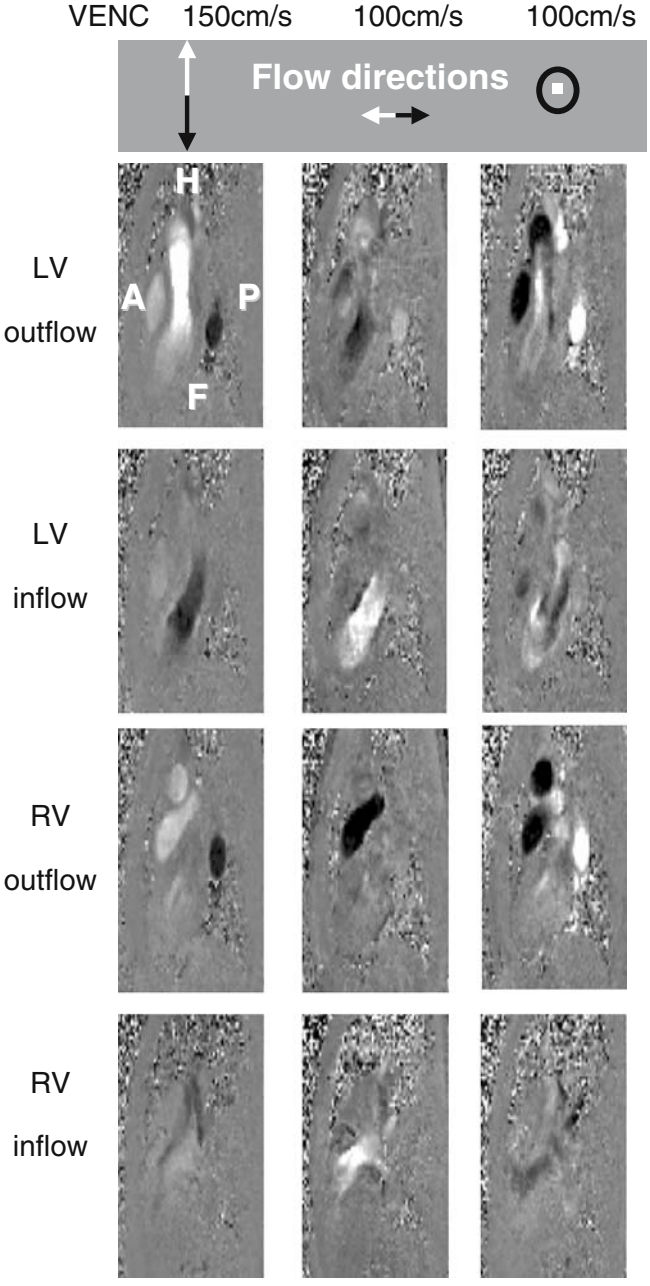

Fig. 9 Three-directional three-dimensional cine flow acquisition of entire heart and great vessels. Selected systolic frames and slices showing ventricular outflow and inflow patterns. The image planes in this normal subject are near sagittal

improve understanding of the asymmetries and some circulatory "tuning" [51, 52] or for computational fluid dynamics.

"Real-time" flow imaging

Avoiding breath-holding, "real-time" images in each cardiac cycle are also less vulnerable to arrhythmia. A range of new applications in short-term flow variations has been investigated, e.g. reactive hyperemia in peripheral vessels after releasing a pressure cuff occlusion [53], exercise testing [54], and in pediatric congential shunt flow [55] enabling manoeuvres as used during ultrasound velocity measurements. Real-time imaging has coarser spatial and temporal resolutions than slower MRI methods [56].

Coronary artery blood flow (CBF)

The difficulties associated with CBF arise from their smallness, tortuous pathways and motion with both the cardiac and respiratory cycles. These problems are compounded by epicardial fat surrounding the arteries. The rhythmic squeezing of the arteries as the heart contracts and the cyclic changes in aortic pressure result in phasic temporal flow profiles, with systolic and early diastolic peaks. Resting flow rates are typically 90 ml/min and in normal subjects, may increase by a factor of 4–5 with pharmacological stress. Peak flow velocity is typically <25 cm/s.

CBF assessment generally uses breath-hold view-shared segmented FLASH phase contrast. However, the long acquisition window (typically 100–140 ms) may result in considerable blurring by cardiac motion and studies have been confined to the left coronary artery, which is less mobile than the right [57]. The absence of fat suppression (necessitated by view-sharing) results in poor vessel contrast at times of slow flow and can also cause increased partial volume effects at edge pixels, which may be reduced by implementing complex-difference, rather than phase difference, processing. Correction for the through-plane motion of the vessel itself is generally performed by subtracting the velocity of an area of adjacent myocardium. For the left coronary artery, this results in the expected diastolic flow predominance [58]. Although studies have reported reasonably good correlations (r=0.7–0.9) between MR and Doppler data, breath-hold segmented FLASH underestimates velocities, with values being typically only 30–40% of those measured by Doppler [58, 59]. Reducing the acquisition window increases accuracy [59] (Fig. 10) but the study takes longer, which poses a particular problem for the use of pharmacological stress. Interleaved spiral phase contrast [60] has a short acquisition window (10 ms), reduces blurring from cardiac motion, allows effective fat suppression and shows the vessel with good contrast throughout the cycle, and is also suitable for the more mobile right coronary arteries. Furthermore, the fine temporal resolution (typically 20–30 ms) can investigate velocity waveforms (Fig. 10), which are known to change with atherosclerotic disease state.

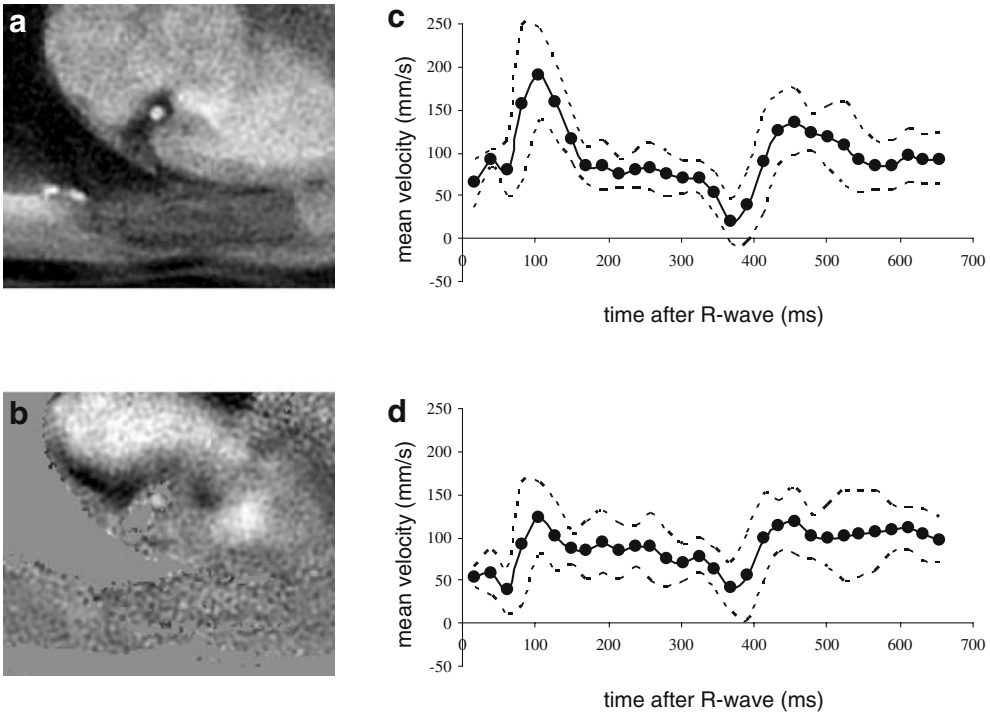

Fig. 10 Diastolic magnitude (**a**) and phase images (**b**) of a right coronary artery in a healthy volunteer. **c, d** Mean (±SD) flow waveforms in five healthy subjects before (**c**) and after (**d**) correction for through-plane motion of the vessel

Due to their larger diameter and their extracardiac course, CBF assessment can be done in coronary bypass grafts as well. Examinations under rest and adenosine stress enable the determination of flow reserves and thus the detection of hemodynamically significant graft stenosis. Langerak et al. [61] showed that this combined assessment was successful in 80% (104/130) of all evaluated bypass grafts. Using a multivariate analysis of the parameters mean flow velocity, peak systolic and diastolic velocity and coronary flow reserve, they were able to detect >70% stenoses in sequential and singular vein grafts with sensitivities of 94 and 96% and specificities of 71% and 92%, respectively. The same working group demonstrated a significant increase of mean flow and coronary flow reserve after PTCA [62].

Vessel wall shear stress (WSS)

Vessel wall shear stress is important in understanding and assessing vulnerability of atherosclerotic plaque. Phase-contrast cines determine WSS using the flow profile as a function of position across the lumen to estimate the velocity gradient at the wall [63]. Recent clinical research includes estimates of WSS during the cardiac cycle in healthy pulmonary artery and in Fontan patients where flow was reduced and WSS increased [64]. Comparison studies suggest a nonuniform distribution of WSS throughout the arterial system [65] and show alterations during exercise [66]. Phase contrast can also define flow boundary conditions for computational fluid dynamics calculations of WSS and its oscillation during the cycle.

Pulse wave velocity (PWV)

Vessel compliance (distensibility) is affected by wall disease, and can be calculated from the vessel's measured expansion with knowledge of the local pressure change, a difficult limitation for non-invasive work. Compliance also affects the speed of a pressure wave along a vessel, which travels much faster than the blood itself. Cine velocity images at very fine temporal resolution can measure the time of the pulse's arrival at multiple locations down the vessel, so that the PWV can be calculated [67] (among other MRI methods) for PWV [68]). Age-related regional aortic PWV changes [67] have recently been demonstrated in more detail [69], and a study in atherosclerosis showed elevated PWV and other velocity waveform effects of lowered compliance [70].

Myocardial wall velocity

During cardiac contraction and filling, the myocardial wall velocities reach about 10–15 cm/s. To measure these, phase-contrast requires a much narrower VENC than is used even for coronary artery blood flow. As explained earlier, the large and varying phase shifts cause flow artefacts from fast moving material in the velocity-encoded image. Most of the artefacts come from the blood, which can be suppressed by a presaturation method [71]. High velocity sensitivity in multiple directions in a single breathhold demands the fastest phase-contrast imaging sequences. Direct quantification and visualization of velocity has been employed, but other quantitative indices can be derived from myocardial velocity data, most usefully the three-dimensional strain rate. As all three orthogonal components of velocity can be measured, radial, circumferential and longitudinal strain rate tensors can be shown [72, 73] (Fig. 1). Myocardial velocity mapping is yet to be adopted in the clinical environment due to its limited spatial and temporal resolution, and is currently applied to fundamental physiological and clinical research.

References

1. Varaprasathan GA, Araoz PA, Higgins CB, Reddy GP (2002) Quantification of flow dynamics in congenital heart disease: applications of velocity-encoded cine MR imaging. Radiographics 22:895–905
2. Tan RS, Mohiaddin RH (2001) Cardiovascular applications of magnetic resonance flow measurement. Rays 26:71–91 (Review)
3. Lotz J, Meier C, Leppert A, Galanski M (2002) Cardiovascular flow measurement with phase-contrast MR imaging: basic facts and implementation. Radiographics 22:651–671
4. Greil G, Geva T, Maier SE, Powell AJ (2002) Effect of acquisition parameters on the accuracy of velocity encoded cine magnetic resonance imaging blood flow measurements. J Magn Reson Imaging 15:47–54
5. Powell AJ, Tsai-Goodman B, Prakash A, Greil GF, Geva T (2003) Comparison between phase-velocity cine magnetic resonance imaging and invasive oximetry for quantification of atrial shunts. Am J Cardiol 15:1523–1525
6. Reimer P, Boos M (1999) Phase-contrast MR angiography of peripheral arteries: technique and clinical application. Eur Radiol 9:122–127
7. Markl M, Bammer R, Alley MT, Elkins CJ, Draney MT, Barnett A, Moseley ME, Glover GH, Pelc NJ (2003) Generalized reconstruction of phase contrast MRI: analysis and correction of the effect of gradient field distortions. Magn Reson Med 50:791–801

8. Ding S, Wolff SD, Epstein FH (1998) Improved coverage in dynamic contrast-enhanced cardiac MRI using interleaved gradient-echo EPI. Magn Reson Med 39:514–519
9. Nayak KS, Hu BS, Nishimura DG (2003) Rapid quantitation of high-speed flow jets. Magn Reson Med 50:366–372
10. Beerbaum P, Korperich H, Gieseke J, Barth P, Peuster M, Meyer H (2003) Rapid left-to-right shunt quantification in children by phase-contrast magnetic resonance imaging combined with sensitivity encoding (SENSE). Circulation 108:1355–1361
11. Markl M, Schneider B, Hennig J (2002) Fast phase contrast cardiac magnetic resonance imaging: improved assessment and analysis of left ventricular wall motion. J Magn Reson Imaging 15:642–653
12. Scheffler K, Lehnhardt S (2003) Principles and applications of balanced SSFP techniques. Eur Radiol 13:2409–2418
13. Bernstein MA, Zhou XJ, Polzin JA, King KF, Ganin A, Pelc NJ, Glover GH (1998) Concomitant gradient terms in phase contrast MR: analysis and correction. Magn Reson Med 39:300–308
14. Tang C, Blatter DD, Parker DL (1993) Accuracy of phase-contrast flow measurements in the presence of partial-volume effects. J Magn Reson Imaging 3:377–385
15. Hamilton CA, Moran PR, Santago P II, Rajala SA (1994) Effects of intravoxel velocity distributions on the accuracy of the phase-mapping method in phase-contrast MR angiography. J Magn Reson Imaging 4:752–755
16. Chatzimavroudis GP, Zhang H, Halliburton SS, Moore JR, Simonetti OP, Schvartzman PR, Stillman AE, White RD (2003) Clinical blood flow quantification with segmented k-space magnetic resonance phase velocity mapping. J Magn Reson Imaging 17:65–71
17. Laffon E, Lecesne R, De Ledinghen V, Valli N, Couzigou P, Laurent F, Drouillard J, Ducassou D, Barat JL (1999) Segmented 5 versus nonsegmented flow quantitation: comparison of portal vein flow measurements. Invest Radiol 34:176–180
18. de Haan MW, Kouwenhoven M, Kessels AG, van Engelshoven JM (2000) Renal artery blood flow: quantification with breath-hold or respiratory triggered phase-contrast MR imaging. Eur Radiol 10:1133–1137
19. Arheden H, Saeed M, Tornqvist E, Lund G, Wendland MF, Higgins CB, Stahlberg F (2001) Accuracy of segmented MR velocity mapping to measure small vessel pulsatile flow in a phantom simulating cardiac motion. J Magn Reson Imaging 13:722–728
20. van den Hout RJ, Lamb HJ, van den Aardweg JG, Schot R, Steendijk P, van der Wall EE, Bax JJ, de Roos A (2003) Real-time MR imaging of aortic flow: influence of breathing on left ventricular stroke volume in chronic obstructive pulmonary disease. Radiology 229:513–519
21. Sakuma H, Kawada N, Kubo H, Nishide Y, Takano K, Kato N, Takeda K (2001) Effect of breath holding on blood flow measurement using fast velocity encoded cine MRI. Magn Reson Med 45:346–348
22. Firmin DN, Nayler GL, Kilner PJ, Longmore DB (1990) The application of phase shifts in NMR for flow measurement. Magn Reson Med 14:230–241
23. Thunberg P, Wigstrom L, Wranne B, Engvall J, Karlsson M (2000) Correction for acceleration-induced displacement artifacts in phase contrast imaging. Magn Reson Med 43:734–738
24. Oshinski JN, Ku DN, Bohning DE, Pettigrew RI (1992) Effects of acceleration on the accuracy of MR phase velocity measurements. J Magn Reson Imaging 2:665–670
25. Buonocore MH (1993) Blood flow measurement using variable velocity encoding in the RR interval. Magn Reson Med 29:790–795
26. Wang ZJ, Reddy GP, Gotway MB, Yeh BM, Higgins CB (2003) Cardiovascular shunts: MR imaging evaluation. Radiographics 23 (Special):S181–S194
27. Powell AJ, Tsai-Goodman B, Prakash A, Greil GF, Geva T (2003) Comparison between phase-velocity cine magnetic resonance imaging and invasive oximetry for quantification of atrial shunts. Am J Cardiol 91:1523–1525
28. Kramer U, Dornberger V, Fenchel M, Stauder N, Claussen CD, Miller S (2003) Scimitar syndrome: morphological diagnosis and assessment of hemodynamic significance by magnetic resonance imaging. Eur Radiol 13 (Suppl 4):L147–L150
29. Li W, Davlouros PA, Kilner PJ, Pennell DJ, Gibson D, Henein MY, Gatzoulis MA (2004) Doppler-echocardiographic assessment of pulmonary regurgitation in adults with repaired tetralogy of Fallot: comparison with cardiovascular magnetic resonance imaging. Am Heart J 147:165–172
30. Didier D, Ratib O, Lerch R, Friedli B (2000) Detection and quantification of valvular heart disease with dynamic cardiac MR imaging. Radiographics 20:1279–1301
31. Chatzimavroudis GP, Walker PG, Oshinski JN, Franch RH, Pettigrew RI, Yoganathan AP (1997) Slice location dependence of aortic regurgitation measurements with MR phase velocity mapping. Magn Reson Med 37:545–551
32. Reid SA, Walker PG, Fisher J, Nagy Z, Ridgway JP, Watterson KG, Sivananthan MU (2002) The quantification of pulmonary valve haemodynamics using MRI. Int J Card Imaging 18:217–225
33. Kozerke S, Schwitter J, Pedersen EM, Boesiger P (2001) Aortic and mitral regurgitation: quantification using moving slice velocity mapping. J Magn Reson Imaging 14:106–112
34. Oshinski JN, Parks WJ, Markou CP, Bergman HL, Larson BE, Ku DN, Mukundan S Jr, Pettigrew RI (1996) Improved measurement of pressure gradients in aortic coarctation by magnetic resonance imaging. J Am Coll Cardiol 28:1818–1826
35. Henk CB, Grampp S, Koller J, Schoder M, Frank H, Klaar U, Gomischek G, Mostbeck GH (2002) Elimination of errors caused by first-order aliasing in velocity encoded cine-MR measurements of postoperative jets after aortic coarctation: in vitro and in vivo validation. Eur Radiol 12:1523–1531
36. Kilner PJ, Firmin DN, Rees RS, Martinez J, Pennell DJ, Mohiaddin RH, Underwood SR, Longmore DB (1991) Valve and great vessel stenosis: assessment with MR jet velocity mapping. Radiology 178:229–235
37. Konen E, Merchant N, Provost Y, McLaughlin PR, Crossin J, Paul NS (2004) Coarctation of the aorta before and after correction: the role of cardiovascular MRI. Am J Roentgenol 182:1333–1339

38. Sondergaard L, Stahlberg F, Thomsen C (1999) Magnetic resonance imaging of valvular heart disease. J Magn Reson Imaging 10:627–638
39. Holmvang G, Palacios IF, Vlahakes GJ, Dinsmore RE, Miller SW, Liberthson RR, Block PC, Ballen B, Brady TJ, Kantor HL (1995) Imaging and sizing of atrial septal defects by magnetic resonance. Circulation 92:3473–3480
40. Keegan J, Gatehouse PD, John AS, Mohiaddin RH, Firmin DN (2003) Breath-hold signal-loss sequence for the qualitative assessment of flow disturbances in cardiovascular MR. J Magn Reson Imaging 18:496–501
41. Storey P, Li W, Chen Q, Edelman RR (2004) Flow artifacts in steady-state free precession cine imaging. Magn Reson Med 51:115–122
42. Strotzer M, Aebert H, Lenhart M, Nitz W, Wild T, Manke C, Volk M, Feuerbach S (2000) Morphology and hemodynamics in dissection of the descending aorta. Assessment with MR imaging. Acta Radiol 41:594–600
43. Kunz RP, Oberholzer K, Kuroczynski W, Horstick G, Krummenauer F, Thelen M, Kreitner KF (2004) Assessment of chronic aortic dissection: contribution of different ECG-gated breath-hold MRI techniques. Am J Roentgenol 182:1319–1326
44. Mousseaux E, Tasu JP, Jolivet O, Simonneau G, Bittoun J, Gaux JC (1999) Pulmonary arterial resistance: noninvasive measurement with indexes of pulmonary flow estimated at velocity-encoded MR imaging-preliminary experience. Radiology 212:896–902
45. Paelinck BP, Lamb HJ, Bax JJ, Van der Wall EE, de Roos A (2002) Assessment of diastolic function by cardiovascular magnetic resonance. Am Heart J 144:198–205
46. Schoenberg SO, Knopp MV, Bock M, Kallinowski F, Just A, Essig M, Hawighorst H, Schad L, van Kaick G (1997) Renal artery stenosis: grading of hemodynamic changes with cine phase-contrast MR blood flow measurements. Radiology 203:45–53
47. Laffon E, Jimenez M, Latrabe V, Ducassou D, Choussat A, Marthan R, Laurent F (2004) Quantitative MRI comparison of systemic hemodynamics in Mustard/Senning repaired patients and healthy volunteers at rest. Eur Radiol 14:875–880
48. Laffon E, Galy-Lacour C, Laurent F, Ducassou D, Marthan R (2003) MRI quantification of the role of the reflected pressure wave on coronary and ascending aortic blood flow. Physiol Meas 24:681–692
49. Bogren HG, Buonocore MH, Valente RJ (2004) Four-dimensional magnetic resonance velocity mapping of blood flow patterns in the aorta in patients with atherosclerotic coronary artery disease compared to age-matched normal subjects. J Magn Reson Imaging 19:417–427
50. Kozerke S, Hasenkam JM, Pedersen EM, Boesiger P (2001) Visualization of flow patterns distal to aortic valve prostheses in humans using a fast approach for cine 3D velocity mapping. J Magn Reson Imaging 13:690–698
51. Kilner PJ, Yang GZ, Wilkes AJ, Mohiaddin RH, Firmin DN, Yacoub MH (2000) Asymmetric redirection of flow through the heart. Nature 404:759–761
52. Laffon E, Bernard V, Montaudon M, Marthan R, Barat JL, Laurent F (2001) Tuning of pulmonary arterial circulation evidenced by MR phase mapping in healthy volunteers. J Appl Physiol 90:469–474
53. Mohiaddin RH, Gatehouse D, Moon JC, Youssuffidin M, Yang GZ, Firmin DN, Pennell DJ (2002) Assessment of reactive hyperaemia using real time zonal echo-planar flow imaging. J Cardiovasc Magn Reson 4:283–287
54. Hjortdal VE, Emmertsen K, Stenbog E, Frund T, Schmidt MR, Kromann O, Sorensen K, Pedersen EM (2003) Effects of exercise and respiration on blood flow in total cavopulmonary connection: a real-time magnetic resonance flow study. Circulation 108:1227–1231
55. Korperich H, Gieseke J, Barth P, Hoogeveen R, Esdorn H, Peterschroder A, Meyer H, Beerbaum P (2004) Flow volume and shunt quantification in pediatric congenital heart disease by real-time magnetic resonance velocity mapping: a validation study. Circulation 109:1987–1993
56. Klein C, Schalla S, Schnackenburg B, Bornstedt A, Fleck E, Nagel E (2001) Magnetic resonance flow measurements in real time: comparison with a standard gradient-echo technique. J Magn Reson Imaging 14:306–310
57. Hofman MB, Wickline SA, Lorenz CH (1998) Quantification of in-plane motion of the coronary arteries during the cardiac cycle: implications for acquisition window duration for MR flow quantification. J Magn Reson Imaging 8:568–576
58. Shibata M, Sakuma H, Isaka N, Takeda K, Higgins CB, Nakano T (1999) Assessment of coronary flow reserve with fast cine phase contrast magnetic resonance imaging: comparison with measurement by Doppler guidewire. J Magn Reson Imaging 10:563–568
59. Nagel E, Bornstedt A, Hug J, Schnackenburg B, Wellnhofer E, Fleck E (1999) Noninvasive determination of coronary blood flow velocity with magnetic resonance imaging: comparison of breath-hold and navigator techniques with intravascular ultrasound. Magn Reson Med 41:544–549
60. Keegan J, Gatehouse PD, Mohiaddin RH, Yang GZ, Firmin DN (2004) Comparison of spiral and FLASH phase velocity mapping, with and without breath-holding, for the assessment of left and right coronary artery blood flow velocity. J Magn Reson Imaging 19:40–49
61. Langerak SE, Vliegen HW, Jukema JW, Kunz P, Zwinderman AH, Lamb HJ, van der Wall EE, de Roos A (2003) Value of magnetic resinance imagng for the noninvasive detection of stenosis in coronary artery bypass grafts and recipient coronary arteries. Circulation 107:1502–1508
62. Langerak SE, Vliegen HW, Jukema JW, Zwinderman AH, Lamb HJ, de Roos A, van der Wall EE (2003) Vein graft function improvement after percutaneous intervention: evaluation with MR flow mapping. Radiology 228:834–841
63. Masaryk AM, Frayne R, Unal O, Krupinski E, Strother CM (1999) In vitro and in vivo comparison of three MR measurement methods for calculating vascular shear stress in the internal carotid artery. Am J Neuroradiol 20 237–245
64. Morgan VL, Graham TP Jr, Roselli RJ, Lorenz CH (1998) Alterations in pulmonary artery flow patterns and shear stress determined with three-dimensional phase-contrast magnetic resonance imaging in Fontan patients. J Thorac Cardiovasc Surg 116:294–304
65. Wu SP, Ringgaard S, Oyre S, Hansen MS, Rasmus S, Pedersen EM (2004) Wall shear rates differ between the normal carotid, femoral, and brachial arteries: an in vivo MRI study. J Magn Reson Imaging 19:188–193
66. Cheng CP, Herfkens RJ, Taylor CA (2003) Inferior vena caval hemodynamics quantified in vivo at rest and during cycling exercise using magnetic resonance imaging. Am J Physiol Heart Circ Physiol 284 H1161–H1167
67. Mohiaddin RH, Firmin DN, Longmore DB (1993) Age-related changes of human aortic flow wave velocity measured noninvasively by magnetic resonance imaging. J Appl Physiol 74:492–497
68. Vulliemoz S, Stergiopulos N, Meuli R (2002) Estimation of local aortic elastic properties with MRI. Magn Reson Med 47:649–654

69. Rogers WJ, Hu YL, Coast D, Vido DA, Kramer CM, Pyeritz RE, Reichek N (2001) Age-associated changes in regional aortic pulse wave velocity. J Am Coll Cardiol 38:1123–1129
70. Nesbitt E, Schmidt-Trucksass A, Il'yasov KA, Weber H, Huonker M, Laubenberger J, Keul J, Hennig J, Langer M (2000) Assessment of arterial blood flow characteristics in normal and atherosclerotic vessels with the fast Fourier flow method. MAGMA 10:27–34
71. Drangova M, Zhu Y, Pelc N (1997) Effect of artifacts due to flowing blood on the reproducibility of phase-contrast measurements of myocardial motion. J Magn Reson Imaging 7:664–668
72. Wedeen V (1992) Magnetic Resonance Imaging of myocardial kinematics, technique to detect, localize, and quantify the strain rates of the active human myocardium. Mag Res Med 27:52–67
73. Masood S, Gao J, Yang G (2002) Virtual tagging: numerical considerations and phantom validation. IEEE Trans Med Imag 21:1123–1131